

Synthesis and study of new functionalized silica aerogel–poly(methyl methacrylate) composites for biomedical use

**István Lázár^{a*}, Helga Fruzsina Bereczki^a, Sándor Manó^b, Lajos Daróczy^c, György Deák^d, István Fábán^a,
Zoltán Csernátóy^b**

^a Department of Inorganic and Analytical Chemistry, University of Debrecen,

Egyetem tér 1, Debrecen, Hungary, 4032,

^b Department of Orthopaedic Surgery, University of Debrecen,

Nagyerdei krt. 98, Debrecen, Hungary, 4012

^c Department of Solid State Physics, University of Debrecen,

Bem tér 18, Debrecen, Hungary, 4032

^d Department of Applied Chemistry, University of Debrecen,

Egyetem tér 1, Debrecen, Hungary, 4032

* Corresponding author. Tel.: +36 52 512900 22376, fax: +36 52 518660,

E-mail address: lazar@science.unideb.hu

Synthesis and study of new functionalized silica aerogel–poly(methyl methacrylate) composites for biomedical use

István Lázár^{a*}, Helga Fruzsina Bereczki^a, Sándor Manó^b, Lajos Daróczy^c, György Deák^d, István Fábián^a, Zoltán Csernátóny^b

^a Department of Inorganic and Analytical Chemistry, University of Debrecen, Egyetem tér 1, Debrecen, Hungary, 4032,

^b Department of Orthopaedic Surgery, University of Debrecen, Nagyerdei krt. 98, Debrecen, Hungary, 4012

^c Department of Solid State Physics, University of Debrecen, Bem tér 18, Debrecen, Hungary, 4032

^d Department of Applied Chemistry, University of Debrecen, Egyetem tér 1, Debrecen, Hungary, 4032

* Corresponding author. Tel.: +36 52 512900 22376, fax: +36 52 518660, E-mail address:

lazar@science.unideb.hu

ABSTRACT

Monolithic silica aerogels are nanostructured solids characterized with exceptionally high porosity and specific surface area. Although their strength can be improved by surface treatment with polymers, none of them has been tested yet as a filler in biocompatible polymer composites. The new aerogel–poly(methyl methacrylate) composites were prepared by free radical bulk polymerization of neat methyl methacrylate in the presence of natural and functionalized silica aerogels at 60 °C, using cumene hydroperoxide initiator and 4,N,N-trimethyl-aniline redox pair. Synthetic conditions were set to be most similar to the setting of orthopedic bone cements. Structures, compositions, and molecular weight distributions were determined by scanning electron microscopy, combustion analysis and gel permeation chromatography, respectively. Compressive strength, Shore D hardness and Gardner's impact strength were measured, and the fracture properties were compared to the matrices. All four aerogel fillers resulted in significant enhancement in compressive strength, reaching a maximum value of 123 MPa. Dissolution of H103PC-1 natural and H106PB-1 C16 modified aerogel containing specimens in simulated body fluid occurred in twenty days, leaving porous surfaces behind, which may give rise to higher tissue adhesion potential in bone cements. Heat treated silica aerogel in H112PA-1 showed no leaching out, and its composites might be usefull in high-load technical applications.

1. Introduction

Poly(methyl methacrylate) (PMMA) is widely used in almost all areas of science and industry from transparent window applications, surface coatings and architecture to biomechanical materials, tissue engineering [1,2] and controlled-release drug-delivery systems [3,4]. In orthopedic surgery, for example, a significant portion of bone cements currently in use are either copolymers or organic/inorganic composites of poly(methyl methacrylate) [5–7] or its hydrophilic derivatives [8]. In dentistry, the major organic component of denture materials and white dental fillings is PMMA [9,10]. Improving the mechanical properties, hardness, impact resistance, heat resistance, and preserving transparency are important goals of PMMA research today. For biomedical applications, additional requirements like biocompatibility and tissue compatibility [11] or characteristic behavior under physiological conditions [12] are also addressed.

Combining organic PMMA matrix with inorganic nano-fillers may lead to significant improvement in heat resistance [13], mechanical strength, wettability, etc. [14]. The number of fillers that have been used for such purposes is fairly high, including nano-silica particles [15,16], nano-titania [17], carbon nanotubes [18], nano-clays [19], hydroxyapatite [20], nano-calcium carbonate [21], organomodified montmorillonite [22] or glass microbeads [23]. Surface modified nano-silica–PMMA composites showed increased thermal stability, which was attributed to the free radical blocking (shielding) effect of the silica nanoparticles [15,24].

Certain alkoxy-silanes (dental silanes) are extensively used as organofunctional coupling agents in dental materials to increase adhesion between the polymeric matrix and the guest particles [25]. Sol-gel derived silicas drew significant attention in biomaterials and bone tissue regeneration research in the last decade [26]. Embedding of mesoporous silica nanoparticles (MSNs) in commercially available acrylic bone cement increased the compressive strength and modulus of the cement, but decreased the flexural strength and fracture toughness [27].

Biocompatible amorphous silica nanoparticles provided significant improvement in both short-term and long-term mechanical strength of calcium phosphate bone cement, soaked in a physiological solution [28].

Silica aerogels are among the lowest bulk density solids in the world characterized by unique properties like extremely low thermal conductivity, very high specific surface area and the best sound attenuation among solids [29]. They are synthesized typically from alkoxy-silanes by hydrolysis and polycondensation forming a jelly, which is then dried under supercritical conditions to preserve the original structure [30,31].

Medium and low density silica aerogels are fragile materials, but their structure can be reinforced very significantly with polymeric surface layers in the nanometer range [32]. Aerogels are very sensitive to any kind of wetting liquids, and their contact leads to rapid collapse of the monolithic structure. Recently it has been demonstrated that the collapse stops at the multi-micron level, and the resulting particles are mechanically strong enough to be used as liquid chromatography stationary phases in microchips [33] or in HPLC micro-columns [34,35].

Most recently we have synthesized a series of silica aerogel based new composites containing calcium phosphate and hydroxyapatite particles for artificial bone substitution, in which monolithic silica aerogel framework served as a biocompatible and highly permeable matrix [36,37]. All of them showed significant bioactivity *in vivo*, indicating that silica aerogel can be used successfully in artificial bone materials. The fact that aerogel particles may remain intact on contact with liquids gave rise to the conclusion that their pores can be saturated with biocompatible polymers, which are currently used in the medical practice. Therefore, we have decided to prepare and test the first PMMA-silica aerogel composites, in which the mesoporous particles would serve as a new type of highly porous biocompatible fillers. Here we report the synthetic process, embedding of functionalized silica aerogels in and bulk polymerization of MMA in situ, and present the mechanical and fracture properties, molecular weight distributions, simulated body fluid behavior, and potential applicability of the new PMMA-silica aerogel composite materials.

2. Experimental

Tetramethyl orthosilicate (TMOS), hexadecyl trimethoxysilane (HDTMOS), phenyl trimethoxysilane (PhTMOS), methyl methacrylate (MMA), 4,N,N-trimethyl-aniline (TMA), cumene hydroperoxide (80 %) (CHPO), tris(hydroxymethyl)-aminomethane (tris) and inorganic salts were purchased from Aldrich. MMA was distilled under a nitrogen protecting atmosphere right before its use in order to remove the stabilizer hydroquinone monomethyl ether. Other reactants were used without further purification. Organic solvents (methanol, acetone, tetrahydrofuran, hexane, dimethyl formamide) and ammonia solution were of ACS reagent grade, purchased from VWR Int., Debrecen and Molar Chemicals Ltd., Budapest and used without further purification. Double deionized water was prepared by a MilliQ equipment. Nitrogen gas cylinders (99.995%) and carbon dioxide gas cylinders (Biogon-C, 99.5%) equipped with a dip tube were purchased from Linde Hungary Kft., Hungary.

2.1. Instrumentation and methods

2.1.1. Liquid CO₂ extraction and supercritical drying

Supercritical CO₂ drying was performed in a custom-made high pressure 1.5 L volume stainless steel tank reactor equipped with a mechanical pressure gauge, stainless steel needle valves (all purchased from Linde and Swagelok) and a liquid CO₂ intake manifold. The decompression valve was connected through an empty buffer tube, and a 50 cm long stainless steel capillary (0.18 mm ID) to a dry commercial HPLC column (C18, 4.6 x 150 mm) packed with 5 µm particles, which served as a dynamic flow controller and pressure dampener unit. An electric heating mantle and a water-cooled spiral tube were assembled to the reactor's body to provide controlled temperature changes. Internal temperature was determined by an immersed K-type temperature probe (Fig. 1).

Fig. 1 approx. here

2.1.2. SEM

Scanning electron microscopy studies were performed by a Hitachi S-4300 instrument (SEM) equipped with a Bruker energy dispersive X-ray spectroscope. The monolithic aerogel samples of approximately 2-4 mm sizes were embedded in a low melting point alloy (Wood's metal). Composite samples were scanned directly after fracture. All surfaces were covered by a sputtered gold conductive layer. 5-10 kV accelerating voltage was used for taking the high resolution pictures.

2.1.3. Gel permeation chromatography

For the determination of molecular weights and polydispersity indices a Waters 2695 Separations Module chromatograph equipped with Waters Styragel, HR 0.5, HR 1, HR 2, HR 4, 4.8x300 mm column-bank and a Waters 2414 RI detector were used, both were operated at 35 °C. Tetrahydrofuran (HPLC grade) was used as a mobile phase (0.5 ml/min) and 10 µl volumes of samples were injected. For the calibration polystyrene standards (Merck) were used. The individual samples were dissolved in THF in 10 mg/ml concentration. Number average molar weight (M_n), weight average molar weight (M_w) and polydispersity index (PDI) were defined according to the standard definitions [38] and determined from GPC chromatograms. M_p value indicates the molecular weight belonging to the peak maximum. In lack of the appropriate Mark-Houwink-Sakurada parameters [39,40] for 35 °C temperature, molecular weights are presented without correction (Table 1).

Table 1 approx. here

2.1.4. Mechanical testing

Mechanical tests were performed at the Laboratory of Biomechanics (University of Debrecen). First, a Shore D hardness test was implemented on each specimen. Based on the EN ISO 868:2003 standard, we measured the instantaneous hardness (reading time 0.2 s) on both parallel surfaces of the cylindrical specimens with a D type durometer.

As the next step, we executed compression tests based on the standard ISO 604:2003 using an Instron 8874 servohydraulic material testing machine. The carefully prepared, parallel-ended specimens were placed on the lower compression anvil, then the upper anvil compressed the specimen with the speed of 1 mm/min. During the tests, the system recorded the actual values of the compressive load and extension, as well as the compressive stress and strain based on the exact geometry. The yield stress is the stress of the yield point that is the point of local maximum stress that the sample can withstand. This is the first point of the stress-strain curve, when the stress starts to fall. From the initial linear region of the stress-strain curves the compressive moduli values were calculated by the following formula (Eq. 1):

$$E = \frac{\sigma}{\varepsilon} = \frac{F \cdot L_0}{A_0 \cdot \Delta L} \quad (\text{Eq. 1})$$

where E is the compressive modulus, F is the force applied on the object. A_0 is the original cross-sectional area through which the force is applied, ΔL is the amount by which the length of the object changes. L_0 is the original length of the object.

Impact strengths were determined by a custom-made miniature falling dart impact tester of Gardner's type, equipped with an anti rebound device. The dart (3.00 mm diameter and 6.0 mm long, hemisphere-tipped) was attached to a guided 500 g falling weight. The samples were machined to cylindrical shape of approximately 14 mm diameter and 5-7 mm thickness, and their parallel surfaces were wet-polished to have a smooth surface. Due to the very limited number of specimens, each sample was impacted several times at different points until the sample fractured. New impact points were set to regions free of cracks and crazing. Drop heights leading to complete fracture were recorded. Impact points and cross sections of the fracture impact points were examined by a Zeiss stereo microscope equipped with a polarizing adapter in both reflectance and transmission modes.

2.2. Materials

2.3. Silica aerogels (Si and Si-H)

Two reactant solutions (designated A and B) were prepared in advance. In solution-A the silane reagent TMOS (6.70 mL, 45.4 mmol) was dissolved in methanol (15.7 mL, 388 mmol). Solution-B contained aqueous ammonia solution (6.34 M, 5.00 mL, 31.7 mmol NH₃, H₂O approx. 95 mmol) and water (5.40 mL, 300 mmol) dissolved in methanol (33.6 mL, 0.83 mol). Solutions A and B were mixed using a magnetic stirrer and poured into a PVC plastic mold (the inner surface was lined with PTFE film), and sealed. After 24 h the transparent monolithic alcogel was removed from the mold, transferred into a perforated frame and soaked in an aging solution containing ammonia solution (25%, 20 mL) and water (20 mL) in methanol (60 mL) for two days to reinforce its structure. The aging solution was gradually replaced by methanol, and then by acetone. Acetone was extracted from the gels with a semi-continuous flow of liquid carbon dioxide, then dried under supercritical conditions according to the following general procedure. Wet gel samples were transferred into the supercritical reactor (Fig. 1) filled with 1 L of acetone. After sealing and securing the reactor, a very slight overpressure of carbon dioxide was applied, and acetone was drained through the bottom port. The reactor was charged and kept charged with liquid carbon dioxide, let to stand overnight, then the rest of acetone was carefully drained. The reactor was flushed with a controlled flow of liquid carbon dioxide as long as an acetone-free state had been reached, then all ports were closed, and the temperature raised to 80 °C and kept at this value for the rest of the process. When the internal pressure reached the maximum value (typically between 110 and 150 bars, depending on the charging temperature), the samples were conditioned for at least 2-3 hours. Finally, the reactor was slowly depressurized through porous flow restrictors at a rate of 1 bar/min of pressure drop. When internal overpressure dropped to zero the reactor was purged with argon gas to remove traces of solvent vapors. At the end, the reactor was opened; aerogel monoliths were removed, weighed and stored in tightly closed containers.

2.3.1. Hexadecyl-modified silica aerogel (C16)

Synthesis and supercritical drying was performed as described for silica aerogel with the following modifications. Solution-A contained methanol (9.90 mL), TMOS (2.50 mL, 15.3 mmol) and HDTMOS (0.25 mL, 0.64 mmol). Solution-B was prepared from dimethyl formamide (DMF, 19.8 mL), water (2.50 mL, 139 mmol) and aqueous NH₃ solution (3.30 mL 25 % m/m, containing 44.1 mmol NH₃, 125 mmol H₂O). The reaction mixture was let to set at room temperature for one day, then aged in methanol.

2.3.2. Phenyl-modified silica aerogel (Ph)

Synthesis and supercritical drying was performed as described in the previous paragraphs with the following modifications. Solution-A contained methanol (12.0 mL) TMOS (3.00 mL) and PhTMOS (6,40 mL). Solution-B

was a mixture of water (3.00 mL) and ammonia solution (25%, 2.00 mL) in methanol (12.0 mL). The aging solution contained ammonia solution (25%, 40 mL), water (20 mL) and methanol (300 mL).

2.3.3. Preparation of aerogel-PMMA composites

Approximately 150 mg of a ground and sieved aerogel sample was placed in a standard long test tube, then a PTFE inlet tube was immersed through a one-hole silicone rubber stopper and a glass T-joint. Pesticide grade fine glass wool plug was placed in, to prevent elutriation of the finest particles. The assembly was then connected to the third port of a three-way stopcock. The other two ports were connected to a nitrogen manifold and a two-stage rotary vacuum pump. The sample was gradually evacuated and kept under dynamic vacuum (5 mbar) at 100 °C for 30-60 minutes, then re-pressurized with dry and oxygen-free nitrogen gas. At the beginning aerogel particles fluidized very extensively. The procedure was repeated several times. Finally, the sample was evacuated, kept under static vacuum and the bulk polymerization mixture (freshly prepared from 6.00 mL of MMA, 60 µL of CHPO and 60 µL of TMA under nitrogen atmosphere) was slowly introduced from a disposable syringe through the immersed PTFE tube. The test tube was removed from the assembly, flushed with and then sealed hermetically under nitrogen and kept in an oil bath for 24 h at 60 °C. After polymerization completed the test tube was scratched around with a diamond tipped glass cutter and broke open to liberate PMMA composites. The monoliths were machined to cylindrical form on a lathe. At least two specimens were cut out from each cylinder; one from the upper PMMA part, and one from the bottom composite. The specimens were polished smooth at both ends to provide parallel and transparent surfaces.

2.3.4. Treatment of composites in simulated body fluid (SBF)

SBF solution was freshly made in accordance with a published procedure as follows [41]. For a 0.1 M tris stock solution tris (1.2114 g, 10 mmol) was completely dissolved in water in a volumetric flask and filled up to 100 mL. SBF-A solution was made from NaCl (1.5992 g, 27.36 mmol), KCl (0,0458 g, 0,61 mmol), CaCl₂·2H₂O (0,0731 g, 0,50 mmol), MgCl₂·6H₂O (0,0616 g, 0,30 mmol) and 0,1 M tris stock solution (5.00 mL), all dissolved in water and made up to 100 mL volume. SBF-B solution contained Na₂SO₄ (0,0146 g, 0,10 mmol), NaHCO₃ (0,0717 g, 0,85 mmol), K₂HPO₄ (0,0353 g, 0,20 mmol) and 0.1 M tris stock solution (5.00 mL) dissolved in water and filled up to 100 mL final volume. The pH of SBF-A and SBF-B solutions were set to 7.40±0.02 by 0.1 M HCl solution. Solutions A and B were mixed in equal volumes making SBF test solution directly prior to use. pH of the SBF solution was checked again and set to 7.40±0.02, if necessary.

In vitro bioactivity studies were performed by soaking freshly fractured smaller composite specimens in 4 ml volume of SBF test solution in completely filled-up and sealed sample vials kept at 37 °C in an incubator for 20

days. After that, the SBF solution was drained, and the specimens were rinsed three times with deionized water, once with methanol, and dried in the vial with a dry nitrogen gas stream introduced through a Pasteur pipette at a rate of 5 L/min.

3. Results and discussion

Natural and functionalized silica aerogel monoliths were prepared by an ammonia-catalyzed sol-gel process and received after supercritical CO₂ drying. Impurities and adsorbed materials were removed from one of the natural silica aerogels by heating at 500 °C for 8 h. Modified aerogels were used as prepared (Fig. 2). This process provided very light and nearly transparent monolithic aerogel cylinders, while a previously published procedure gave a denser gel silica glass used also for embedding in a bulk polymerized PMMA matrix [42].

In order to provide similar conditions for the polymerization that are present during the setting of clinical bone cements, a free radical bulk polymerization technique of methyl methacrylate was used, even though the process was very prone to heat run-off and bubble formation under atmospheric conditions, due to the Trommsdorff-Norrish effect (gel effect) [43,44]. First, the aerogel-free polymerization was tested; the natures of the redox pair and the free-radical initiator (benzoyl peroxide, AIBN, cumene hydroperoxide), the reaction temperature and time were varied. Finally we have found cumene hydroperoxide initiator and 4,N,N-trimethyl-aniline redox pair to be the most advantageous for bubble-free bulk polymerization of freshly distilled methyl-methacrylate at 60 °C and 1 bar pressure, under an oxygen-free nitrogen atmosphere.

Fig. 2 approx. here

Aerogels are extremely porous solids, excellent adsorbents, the pores of which can be filled with any wetting liquids. In our experiments, however, mixing of the aerogel particles in the polymerization mixture resulted in extensive bubble formation during the polymerization process and produced solid foam-like samples of low mechanical strength. Optical microscopy monitoring of the wetting process revealed that the aerogel particles had not been saturated completely on a rapid immersion in MMA, but effectively encapsulated air in the middle of the grains. In addition, aerogel particles served as „boiling chips” during the high-temperature run-off period of the process. Post-wetting removal of air from the wetted particles has also failed. We have developed a vacuum-assisted penetration technique, in which dry aerogel samples were carefully evacuated and desorbed at around 100 °C temperature under dynamic vacuum, and then the polymerization mixture was introduced under static vacuum.

By this manner aerogel particles were saturated completely with the reaction mixture. The experimental setup, however, did not allow us to control the particle distribution or degree of compaction, thus the grains settled down spontaneously, resulting in variable silica content in the lower region. After polymerization was completed, machining and polishing resulted in transparent specimens except for H106PA-1, which was translucent (Fig. 3).

Fig. 3 approx. here

Densities of the specimens were calculated from their weight and dimensions and showed in Table 1. Although the lower, aerogel-containing parts are of a bit higher densities, the differences are minor, and the trend is not general. The phenyl-aerogel composite sample H106PA-1, for example, is less dense than its matrix. Sample HP112PA-1 with natural silica aerogel showed the highest density, which can be attributed to the moderately increased bulk density of that aerogel due to previous heat treatment.

The hardness of the aerogel-containing composite samples was of approximately 2-3 units higher than that of the PMMA matrix, but no connection between the chemical composition of aerogel fillers, and the measured value of hardness was found. That may be the consequence of the largely identical microstructure of the natural and functionalized silica skeletons and the nearly identical molecular weights of the polymer matrix. All attempts to find a correlation between Shore D hardness and Young's modulus of the samples by using the formulae published by either Gent [45] or Qi et al. [46] failed.

Fig. 4 approx. here

Compressive strengths were determined on a servohydraulic tester. Compressive load–compressive extension curves with the yield point are given in Fig. 4. All the compressive strength, compressive modulus and impact strength values are listed in Table 1. Strong reinforcing effect was found for all aerogel composites, even when the aerogel content of the samples was very moderate by weight. If we take the very low compressive strengths (less than 0.2 MPa) of the monolithic aerogels into consideration, the given degree of reinforcement is remarkable. Unfortunately, detailed comparison is not possible due to the very different weight ratios of the fillers, which can not be changed or modified by the present technique. The highest compressive strength was measured for heated natural silica aerogel composites and the lowest one for the C16 derivative. Impact strength values have been determined by a miniature falling dart manual impact tester. It has been observed that the impact strength were

lower for natural silica aerogel, and higher for the modified silica aerogel composites. The impact strength is directly influenced, among others, by the mechanical properties of the filler particles, and their surface adhesion to the matrix [47]. Longer alkyl chains increase adhesion and may help distributing impact energy between the PMMA matrix and the filler particles. Natural silica aerogel filler seems to be the least effective, most likely due to the weakest adhesion of PMMA to the most hydrophilic surfaces.

Higher static reinforcing effects of the natural aerogels can be explained by the number of symmetrical tetrahedral $[\text{SiO}_4]$ units in natural aerogels, which provide an efficient way to distribute the load between the connecting tetrahedra through strong covalent bonds. In the organically modified aerogels a number of three-coordinated $\text{O-Si}(-\text{O})(\text{R})-\text{O}$ and two-coordinated $\text{O-Si}(\text{R})(\text{OH})-\text{O}$ units are present. The latter ones may provide additional flexibility to the silica skeleton, as they can rotate to some extent, but decrease the load distribution capability.

Fracture mechanism also differs significantly, depending on the type of aerogel. Figure 6 shows the micrographs of the impacted surface of a H106PB-1 composite specimen. Local melting and plastic flow of PMMA occurred on impact giving rise to the formation of an impact circle only when drop height is low. Although the sample is far from cracking, the tensile circumferential stress is significant, and high number of thin radial crazing occur. These crazing are visible under transillumination, but still invisible in reflected light. Deep impact craters are formed as the drop height was increased. The craters obviously show signs of extended melting and deformation, followed by rapid cooling. The penetrator head compressed the melt, which formed a high rim crater. Initial crazing opened wide and become well visible by a stereo microscope (Fig. 5b). Sometimes, as an indication of approaching the fracture point, radial butterfly crack formed. However, in this paper, butterfly cracks were not considered a complete fracture.

At the fracture point the melt found a different escape route and did not form a rim. Instead, it was released into the fracture space and occasionally bound the split parts together by a bridge. Transient plasticity of the crater's wall may also lead to creep and rupture, as it is shown in Fig. 5d. Typically, the specimens broke in two diagonally, and occasionally they broke in three. In the latter case, the second fracture line is nearly perpendicular to the first one, which is in accordance with the observations presented in the literature [48].

Fig. 5 approx. here

A significant advantage of the aerogel fillers over copolymers is that they increase the thermal stability of the PMMA significantly. In a preliminary study, PMMA and composite parts of H112PA were pressed to an aluminum plate and heated at 200 °C for 10 minutes. While PMMA melted and charred at this temperature fairly rapidly, no melting, and only moderate darkening was observed in the composite. The protecting effect comes from the wall effect, which shields labile chain ends from free radical formation and protects the chains from degradation by steric hindrance [16].

Fracture surfaces were checked by optical microscopy under normal and polarized light. Four different zones under and around the impact crater can be distinguished clearly in the micrographs (Fig. 6a). Zone 1 is the melt zone, which shows a fairly homogeneous structure. Zone 2 is the bifurcation zone, in which crazing were initiated in the solid by the hydrodynamic pressure of the melt, and then crazing propagated and bifurcated, as long as they led to a virtual front of connecting micro cracks. Zone 3 is the major crack zone, where the weakest plane among micro cracks gave rise to the formation of a complete meridional cracking. Zone 4 is formed after that, when the cracked specimen was split open by the progressing impactor head. That zone shows typical shear bands, which are characteristic features of PMMA fracture surfaces. The zones are barely visible in Fig.s 6b and 6d due to the granular structure of the composites.

Fig. 6 approx. here

Averaged bifurcation angles determined from the micrographs for PMMA matrix synthesized without aerogel filler for comparison, H112PA-1, H106PA-1 and H106PB-1 were $35\pm 9^\circ$, $48\pm 24^\circ$, $34\pm 7^\circ$ and $46\pm 14^\circ$, respectively. Both micrographs and the angles show similarities between PMMA and H106PA-1, as well as H112PA-1 and H106PB-1 composites. H106PA-1 behaved more like PMMA, which was the consequence of the nearly complete structural disintegration of the aerogel particles within the matrix, as shown in Fig. 5c. That type of nearly homogeneous dispersion had no effect on crack propagation, and the composite behaved like PMMA under dynamic conditions. Homogeneous structure is also shown by the nearly identical bifurcation angles and lower standard deviations. For comparison, a commercial 6 mm thick Plexiglas sheet was tested and $22\pm 8^\circ$ bifurcation angles were recorded, which agrees well with the 25° value published in the literature [49].

Composites containing larger, and still intact aerogel particles behaved differently. Micrographs show granular fracture surfaces, and barely visible bifurcation lines. The fracture took place in between, rather than across the

structurally very strong aerogel granules, and the initial cracks are frequently diverted in the direction of the weaker PMMA matrix. This is shown quite well by the highly increased bifurcation angle of 48° and 46° , and the very high standard deviations. It is expected from that type of fracture diversion, that synthesis of large sized and homogeneously filled monolithic aerogel-PMMA composites would show exceptional high mechanical strength, and for that purpose structurally reinforced monolithic aerogels might offer a solution [50].

Number-average and weight-average molecular weights were determined for both the aerogel-free upper PMMA matrices and the lower aerogel-PMMA composite parts from each sample. (Table 1) Polydispersity indices in the range of 2.8-3.8 are in accordance with the nature of free radical mechanism, and high molecular weights are consequences of the gel effect occurring during bulk polymerization. Although there might be some connection between the chemical nature of the aerogel and the molecular weight distribution of PMMA matrix, that type of interaction could have not been established so far. Bulk polymerization resulted in much higher weight average molecular weights and similar number average molecular weights for both the neat and the composite parts than the previously published method [42]. The difference is most likely due to several factors. The first is that different initiators and reaction conditions were used. The second is the mode how the initiator was contacted with MMA. The reported process saturated the gel glass surface with the initiator and then applied MMA. In our case, initiator and redox pair were mixed in MMA and the solution was then contacted with the aerogel phase. By this, only a part of the initiator was adsorbed on the different types of silica surfaces, resulting in much less difference in the molecular weights between the PMMA only and the composite parts, than the published procedure. Most likely, that difference in adsorption resulted in deviations in the mechanical properties on the contrary of the identical experimental conditions.

Simulated body fluid (SBF) is generally used to test PMMA-based bone cements and implants for biocompatibility under physiological conditions [51–54]. Formation of an apatite or hydroxyapatite layer on the surface in SBF is considered an indication of bone adhesion potential. However, making the PMMA surface porous is an alternative route to provide good bone tissue adhesion [55]. We have tested the samples for surface changes by soaking them in SBF for 20 days. Figure 7 shows the fracture surfaces before, and figure 8 after SBF treatments.

Fig. 7 and 8 approx. here

It has been found that natural silica aerogel in H103PB and H103PC-1, and C16-functionalized aerogel in H106PB-1 leached out from the fractured surfaces of the specimens leaving spongy tissues and holes behind, as it can be seen in Fig. 8. Phenyl functionalized H106PA-1 did not dissolve at all, which was most likely the consequence of the highly hydrophobic nature of phenyl aerogel particles, as well as the higher steric hindrance of the phenyl groups on the surface. However, no dissolution of the heat-treated natural silica aerogel from the sample H112PA-1 has been observed. The difference between the solubilities of natural and heat treated silica aerogels can be explained by the change of hydration state of silica surface, which is a key factor in the dissolution of amorphous silicas [56]. High-temperature heating of natural silica aerogel led to complete loss of adsorbed water, plus significant condensation of the surface hydroxyl groups. Decreasing number of silanol groups resulted in decreased solubility of the filler aerogel.

4. Conclusions

Natural and functionalized aerogel-PMMA composites were prepared by free radical bulk polymerization under moderate conditions, and showed significantly improved mechanical properties compared to the PMMA matrix. Reinforcing effects of the aerogels are quite remarkable, especially when their very low own compressive strengths and small weight percentages in the composites are considered. Natural silica aerogels made the composites stronger but more brittle, while organically modified aerogels increased the impact resistance. Simulated body fluid treatment of the composites led to dissolution of natural and C16 modified silica aerogels leaving pores behind, while heat-treated silica and phenyl aerogels were practically insoluble. The results clearly show that monolithic silica aerogels are promising and customizable new type of fillers, which might find applications in orthopedic, dental or technical materials in the future.

5. Acknowledgments

Financial support from the Hungarian Research Fund OTKA 76834 is gratefully acknowledged. The work was supported in part by the TÁMOP-4.2.2/B-10/1-2010-0024 and TÁMOP-4.2.2.A-11/1/KONV-2012-0036 project. The project is co-financed by the European Union and the European Social Fund. H. F. B. thanks Richter Gedeon Ltd. for providing PhD scholarship.

References

1. S. Ramakrishna, J. Mayer, E. Wintermantel, and K. W. Leong, *Compos. Sci. Technol.* **61**, 1189 (2001).
2. S.-H. Rhee and J.-Y. Choi, *Key Eng. Mater.* **218-220**, 433 (2002).
3. J. F. Coelho, P. C. Ferreira, P. Alves, R. Cordeiro, A. C. Fonseca, J. R. Góis, and M. H. Gil, *EPMA J.* **1**, 164 (2010).
4. M. Lin, H. Wang, S. Meng, W. Zhong, Z. Li, R. Cai, Z. Chen, X. Zhou, and Q. Du, *J. Pharm. Sci.* **96**, 1518 (2007).
5. T. Miyazaki, C. Ohtsuki, M. Kyomoto, M. Tanihara, A. Mori, and K. Kuramoto, *J. Biomed. Mater. Res. A* **67A**, 1417 (2003).
6. D. Rentería-Zamarrón, D. A. Cortés-Hernández, L. Bretado-Aragón, and W. Ortega-Lara, *Mater. Des.* **30**, 3318 (2009).
7. S. Shinzato, M. Kobayashi, W. F. Mousa, M. Kamimura, M. Neo, Y. Kitamura, T. Kokubo, and T. Nakamura, *J. Biomed. Mater. Res.* **51**, 258 (2000).
8. L. F. Boesel and R. L. Reis, *Prog. Polym. Sci.* **33**, 180 (2008).
9. R. Bholá, S. M. Bholá, H. Liang, and B. Mishra, *Trends Biomater. Artif. Organs* **23**, 129 (2010).
10. S. Deb, *Proc. Inst. Mech. Eng. [H]* **212**, 453 (1998).
11. F. Mammeri, L. Rozes, E. Le Bourhis, and C. Sanchez, *J. Eur. Ceram. Soc.* **26**, 267 (2006).
12. N. W. Elshereksi, S. H. Mohamed, A. Arifin, and Z. A. Mohd Ishak, *J. Phys. Sci.* **20**, 1 (2009).
13. W. Viratyaporn and R. L. Lehman, *J. Therm. Anal. Calorim.* **103**, 267 (2010).
14. A. P. Kumar, D. Depan, N. S. Tomer, and R. P. Singh, *Prog. Polym. Sci.* **34**, 479 (2009).
15. N. García, T. Corrales, J. Guzmán, and P. Tiemblo, *Polym. Degrad. Stab.* **92**, 635 (2007).
16. J. L. Hang Chau, C.-C. Hsieh, Y.-M. Lin, and A.-K. Li, *Prog. Org. Coat.* **62**, 436 (2008).
17. J. G. Lee and S. H. Kim, *Macromol. Res.* **19**, 72 (2011).
18. K.-S. Kim, J.-H. Byun, G.-H. Lee, and S.-J. Park, *Macromol. Res.* **19**, 14 (2011).
19. Y. Mansoori, A. S. V., S. S. Sanaei, M. R. Zamanloo, and I. Gh., *Macromol. Res.* **18**, 1174 (2010).
20. P. Monvisade, P. Siriphannon, R. Jermungnorn, and S. Rattanabodee, *J. Mater. Sci. Mater. Med.* **18**, 1955 (2007).
21. W. Wu, T. He, J. Chen, X. Zhang, and Y. Chen, *Mater. Lett.* **60**, 2410 (2006).
22. A. K. Nikolaidis, D. S. Achilias, and G. P. Karayannidis, *Ind. Eng. Chem. Res.* **50**, 571 (2011).
23. S. Shinzato, T. Nakamura, K. Ando, T. Kokubo, and Y. Kitamura, *J. Biomed. Mater. Res.* **60**, 556 (2002).
24. F.-A. Zhang, D.-K. Lee, and T. J. Pinnavaia, *Polymer* **50**, 4768 (2009).
25. J. P. Matinlinna, L. V. J. Lassila, M. Özcan, A. Yli-Urpo, and P. K. Vallittu, *Int. J. Prosthodont.* **17**, 155 (2004).
26. D. Arcos and M. Vallet-Regí, *Acta Biomater.* **6**, 2874 (2010).
27. J. Slane, J. Vivanco, J. Meyer, H.-L. Ploeg, and M. Squire, *J. Mech. Behav. Biomed. Mater.* **29**, 451 (2014).
28. M. Mohammadi, S. Hesarak, and M. Hafezi-Ardakani, *Ceram. Int.* (2014).
29. V. Gibiat, O. Lefeuvre, T. Woignier, J. Pelous, and J. Phalippou, *J. Non-Cryst. Solids* **186**, 244 (1995).
30. A. Soleimani Dorcheh and M. H. Abbasi, *J. Mater. Process. Technol.* **199**, 10 (2008).
31. J. Fricke and A. Emmerling, *J. Sol-Gel Sci. Technol.* **13**, 299 (1998).
32. N. Leventis, *Acc. Chem. Res.* **40**, 874 (2007).
33. A. Gaspar, A. Nagy, and I. Lazar, *J. Chromatogr. A* **1218**, 1011 (2011).
34. H. F. Bereczki, Synthesis and chromatographic application of silica aerogels functionalized with complexing agents (in Hungarian), MSc Thesis, University of Debrecen, 2010.
35. A. Kuttor, Functionalized aerogels as chromatographic stationary phases - Synthesis and study (in Hungarian), BSc Thesis, University of Debrecen, 2010.

36. I. Lazar and I. Fabian, WO2013061104 (2 May 2013).
37. I. Lázár, S. Manó, Z. Jónás, L. Kiss, I. Fábián, and Z. Csernátony, *Biomech. Hung.* **3**, 151 (2010).
38. *Modern Size-Exclusion Liquid Chromatography: Practice of Gel Permeation and Gel Filtration Chromatography*, 2nd ed (Wiley, Hoboken, N.J, 2009).
39. H. L. Wagner, *J. Phys. Chem. Ref. Data* **14**, 1101 (1985).
40. H. L. Wagner, *J. Phys. Chem. Ref. Data* **16**, 165 (1987).
41. H. Li, Z.-X. Li, H. Li, Y.-Z. Wu, and Q. Wei, *Mater. Des.* **30**, 3920 (2009).
42. X. Li, T. A. King, and F. Pallikari-Viras, *J. Non-Cryst. Solids* **170**, 243 (1994).
43. R. G. W. Norrish and R. R. Smith, *Nature* **150**, 336 (1942).
44. E. Trommsdorff, H. Köhle, and P. Lagally, *Makromol. Chem. Macromol. Chem. Phys.* **1**, 169 (1948).
45. A. N. Gent, *Inst. Rubber Ind. -- Trans.* **34**, 46 (1958).
46. H. J. Qi, K. Joyce, and M. C. Boyce, *Rubber Chem. Technol.* **76**, 419 (2003).
47. L. Sun, R. F. Gibson, F. Gordaninejad, and J. Suhr, *Compos. Sci. Technol.* **69**, 2392 (2009).
48. D. A. Gorham, A. D. Salman, and M. J. Pitt, *Powder Technol.* **138**, (2003).
49. N. Murphy, M. Ali, and A. Ivankovic, *Eng. Fract. Mech.* **73**, 2569 (2006).
50. H. Maleki, L. Durães, and A. Portugal, *J. Non-Cryst. Solids* **385**, 55 (2014).
51. T. Kokubo, H.-M. Kim, and M. Kawashita, *Biomaterials* **24**, 2161 (2003).
52. A. Sugino, T. Miyazaki, G. Kawachi, K. Kikuta, and C. Ohtsuki, *J. Mater. Sci. Mater. Med.* **19**, 1399 (2008).
53. A. Mori, C. Ohtsuki, T. Miyazaki, A. Sugino, M. Tanihara, K. Kuramoto, and A. Osaka, *J. Mater. Sci. Mater. Med.* **16**, 713 (2005).
54. K.-H. Lee and S.-H. Rhee, *Biomaterials* **30**, 3444 (2009).
55. K. W. Lye, H. Tideman, J. C. G. Wolke, M. A. W. Merckx, F. K. C. Chin, and J. A. Jansen, *Clin. Oral Implants Res.* **24**, 100 (2013).
56. L. T. Zhuravlev, *Colloids Surf. Physicochem. Eng. Asp.* **173**, 1 (2000).

Captions

Fig.1. Structural draw of SC-CO₂ extractor used for preparation of aerogel samples.

Fig.2. A hexadecyl-modified silica aerogel (C16) monolith (left) and its SEM microstructure (center). Vacuum-assisted penetration technique followed by bulk polymerization resulted in C16 aerogel-PMMA composite of good optical transparency (right).

Fig.3. Photograph of the specimens used for compressive testing. Suffix 1 or 2 indicate specimens made from either the lower composite or upper PMMA part of the samples, respectively. All samples are transparent except for HP106PA-1, which is translucent (second row, left)

Fig.4. Compressive load–compressive extension curves of the aerogel-PMMA composite specimens. Black triangles indicate yield points. Dimensions of the cylindrical specimens a–d (diameter x height, all in mm) were 12.27x5.76, 12.29x7.79, 11.03x5.38, 10.58x4.72, respectively.

Fig.5. Optical micrographs of impact damages of hexadecyl-modified sample H106PB-1 a) impact circle on the surface after 11 cm drop test, b) impact crater on the surface after 15 cm drop test, c) impactor head placed nearby the impact crater after complete fracture, d) impact crater after 16 cm drop test, with sidewall rupture.

Fig.6. Micrographs of the impact points led to complete fracture, a) PMMA only H103PC-2, b) heat-treated natural H112PA-1, c) phenyl-modified H106PA-1, d) hexadecyl-modified H106PB-1. Scale bar is 1 mm.

Fig.7. SEM micrographs of the fracture surfaces of composite samples containing a) H103PC-1 natural, b) H112PA-1 heat-treated natural, c) H106PA-1 phenyl-modified, and d) H106PB-1 hexadecyl-modified silica aerogels. Scale bars for pictures a–d are 1 μm, 5 μm, 1 μm and 500 nm, respectively.

Fig.8. SEM micrographs of the fracture surfaces of composite samples after 20-day treatment in simulated body fluid. a) H103PC-1, b) H112PA-1, c) H106PA-1, d) H106PB-1. Scale bars for pictures a–d are 50 μm, 100 μm, 50 μm and 20 μm, respectively.

Table 1 Chemical composition, mechanical properties and molecular weight distribution data of neat and aerogel composite PMMA samples

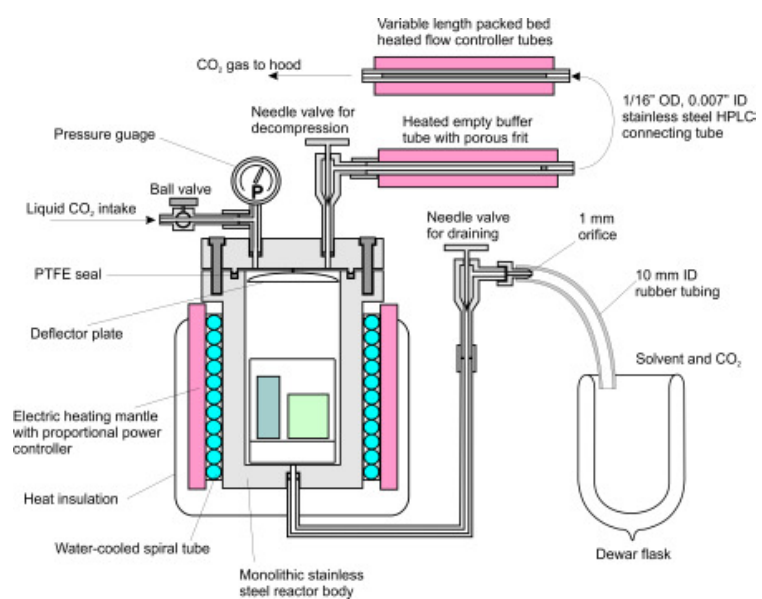


Fig. 1

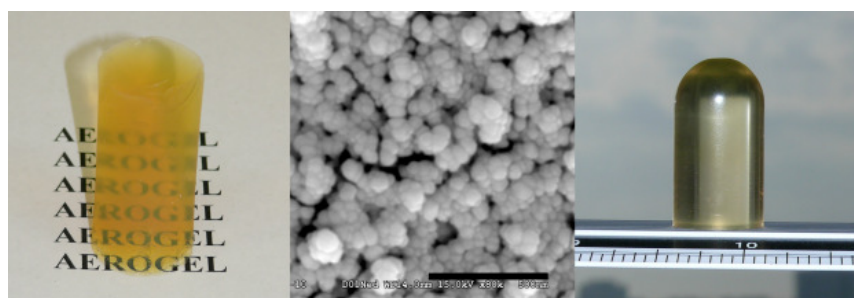


Fig. 2.

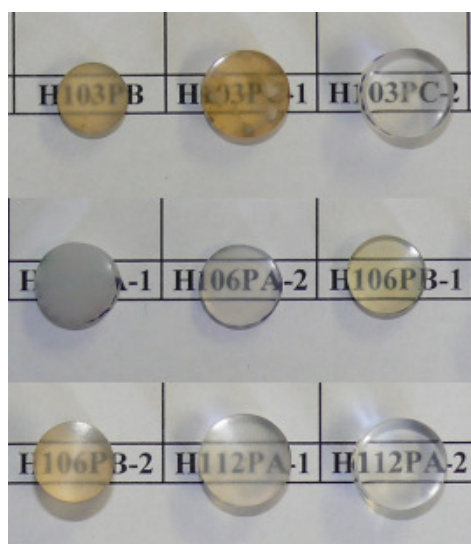


Fig. 3

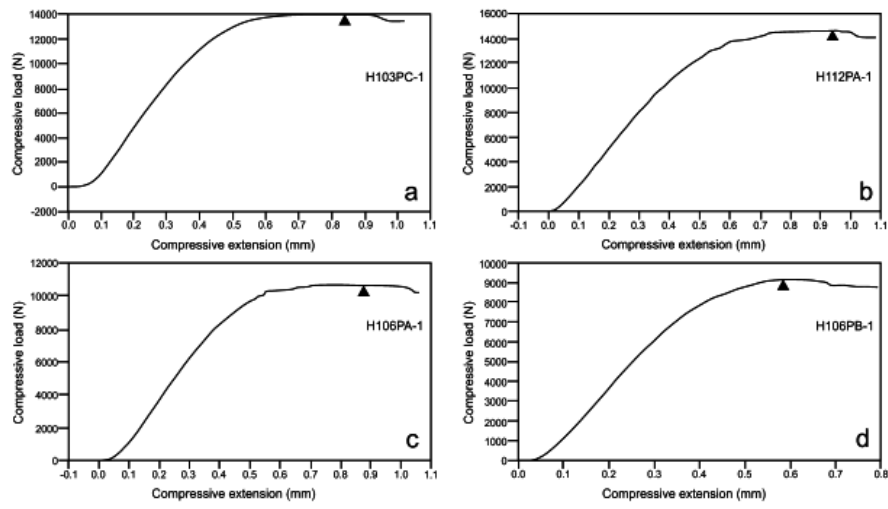


Fig. 4

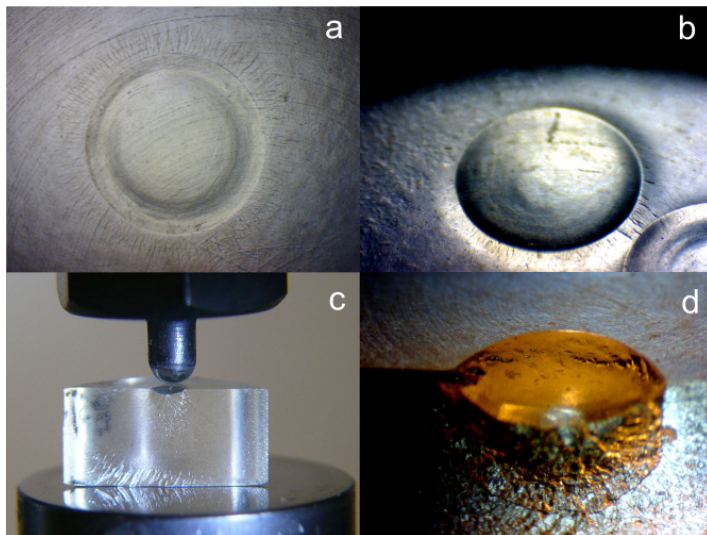


Fig. 5

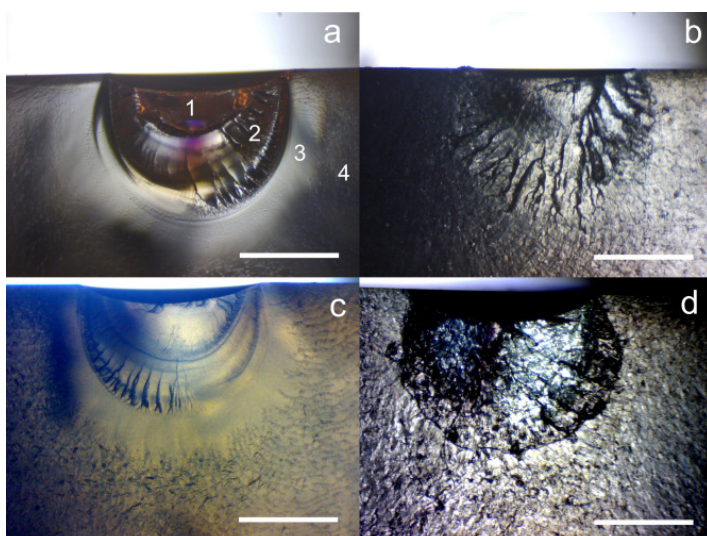


Fig. 6

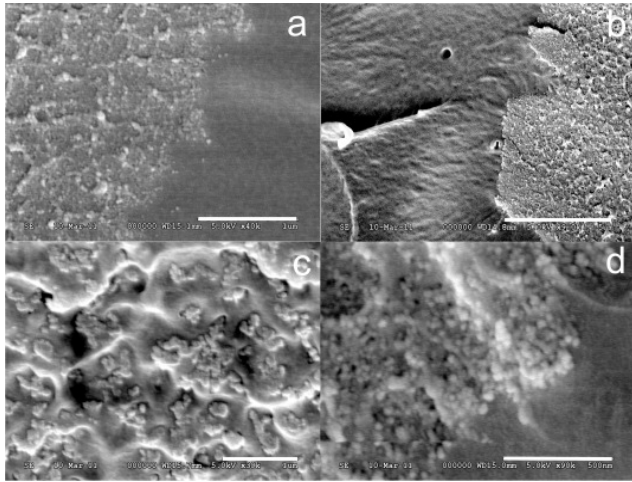


Fig. 7

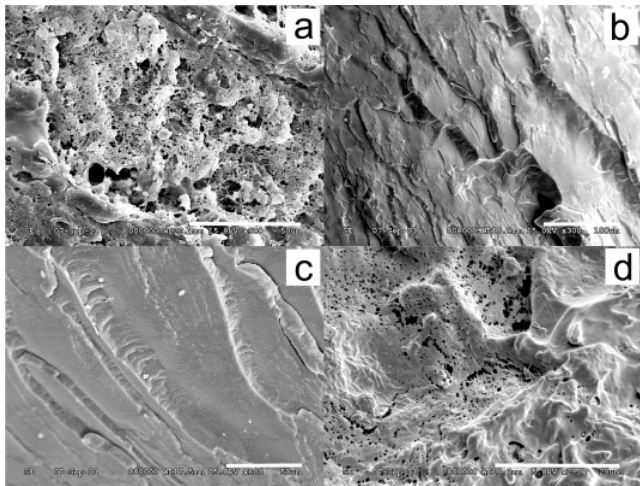


Fig. 8